applied sciences

MDPI

Article

Effect of Vanadium and Rare Earth on the Structure, Phase Transformation Kinetics and Mechanical Properties of Carbide-Free Bainitic Steel Containing Silicon

Behdad Garmeh [1], Masoud Kasiri-Asgarani [1,*], Kamran Amini [2,*], Hamid Ghayour [1], Hamid Reza Bakhsheshi-Rad [1,*] and Filippo Berto [3,*]

[1] Advanced Materials Research Center, Department of Materials Engineering, Najafabad Branch, Islamic Azad University, Najafabad, Iran; Behdad.garmeh@gmail.com (B.G.); hamidghayour70@gmail.com (H.G.)
[2] Center for Advanced Engineering Research, Majlesi Branch, Islamic Azad University, Isfahan, Iran
[3] Department of Mechanical and Industrial Engineering, Norwegian University of Science and Technology, 7491 Trondheim, Norway
* Correspondence: m.kasiri@pmt.iaun.ac.ir (M.K.-A.); k.amini@iaumajlesi.ac.ir (K.A.); rezabakhsheshi@pmt.iaun.ac.ir (H.R.B.-R.); filippo.berto@ntnu.no (F.B.)

Abstract: Carbide-free bainitic (CFB) steels with a matrix of bainitic ferrite and thin layers of retained austenite, to reduce the manufacturing costs, usually do not contain alloying elements. However, a few reports were presented regarding the effect of alloying elements on the properties of these steels. Thus, this study evaluates the effects of vanadium and rare earth (Ce-La) microalloying elements on the structure, phase transformation kinetics, and mechanical properties of carbide-free bainite steel containing silicon fabricated by the casting and austempering procedure. Optical and scanning electron microscopy (OM and SEM), electron backscatter diffraction (EBSD), and X-ray diffraction (XRD) were used to study the microstructure and phase structure. The transformation kinetics were examined by a dilatometry test. Hardness, tensile, and impact tests evaluated the mechanical properties. Due to adding alloying elements, the fracture toughness and change in matrix phases relation was studied by the crack tip opening displacement (CTOD) test and SEM fractography. The microstructure of the silicon added sample was completely carbide-free bainite. The test results showed vanadium helped CFB formation, even in continuous cooling. The primary austenite grain (PAG) size grew by vanadium addition. The EBSD phase map illustrates an increment in the percentage of retained austenite by vanadium. In contrast, the addition of 0.03 wt% rare earth reduced the primary austenite grain size and reduced the retained austenite content. The results of the dilatometry test confirmed that vanadium and rare earth addition both reduced the critical cooling rate of the bainite transformation. Vanadium leads to an earlier cessation of bainite transformation, while rare earth elements postpone this transformation. Mechanical tests showed that the tensile strength of carbide-free bainite steels was strongly influenced by the morphology and volume fraction of austenite. Retained austenite, when transformed to martensite during the transformation-induced plasticity (TRIP) phenomenon, leads to increased tensile strength and fracture toughness, or retained austenite with a film-like shape prevents the growth of cracks by blinding the crack tip. The result of the CTOD test exhibited that retained austenite plays the leading role in increasing crack resistance when TRIP occurs.

Keywords: carbide-free bainite; microalloying; crack tip opening displacement; prior austenite grain size; mechanical properties

Citation: Garmeh, B.; Kasiri-Asgarani, M.; Amini, K.; Ghayour, H.; Bakhsheshi-Rad, H.R.; Berto, F. Effect of Vanadium and Rare Earth on the Structure, Phase Transformation Kinetics and Mechanical Properties of Carbide-Free Bainitic Steel Containing Silicon. *Appl. Sci.* **2022**, *12*, 1668. https://doi.org/10.3390/app12031668

Academic Editor: Ana M. Camacho

Received: 26 November 2021
Accepted: 5 January 2022
Published: 5 February 2022

1. Introduction

Much research has been done since the late 1980s, when a new class of bainite steels with a matrix including bainite ferrite and retained austenite was introduced as nanostructured bainite steels or carbide-free bainite (CFB) steels. These research studies can be

divided into several categories: First, the studies recognizing this phase, among which the most important are those conducted by Sandvik and Nevalainen [1], Caballero and Bhadeshia [2], and Garcia-Mateo and Edmonds [3–6]. The next category includes focusing on the fundamental factors affecting the formation of the carbide-free bainite phase. This category can also be referred to as the joint work of Behadshia and Edmunds. The last category focuses on the behaviors of the CFB phase in different working conditions, such as wear and fatigue [7–9].

Garcia-Mateo et al. [4] exhibited that CFB steels were extended because of their cheap production procedure and good properties. Their result depicted that CFB steels were produced only by adding about 2 wt% of silicon or aluminum via the casting procedure followed by isothermal heat treatment in the low bainite temperature range without the need for thermomechanical work. Adding alloying elements increases the final price of the steel, so studies on the effect of adding alloying elements on the mechanical and structural properties of steel are limited. In this respect, it was exhibited [10] that vanadium could affect the bainitic transformation rate in two ways: the effect on grain size and solute drag. In another study, Sourmail et al. [11] investigated the effect of vanadium on the direct and indirect decomposition of retained austenite. Their result depicted that the addition of vanadium slowed down the austenite decomposition process. In a study by Yu et al. [12], the effect of niobium (Nb) microalloy elements on the thermal stability of carbide-free bainite steel was evaluated. Their result revealed that niobium leads to the higher thermal and mechanical stability of residual austenite films. Niobium improves the morphology of bainite, leading to thinner retained austenite layers.

Conventionally, vanadium, niobium, and titanium alloying elements are used to improve the mechanical properties of steels by precipitation hardening. Vanadium usually results in fine-grained steels by forming carbide in the high-temperature range of Ac3 and preventing the movement of grain boundaries (pinning). However, this phenomenon occurs only in perlite and ferrite steels [13–16] and in bainite and martensite steels; carbide deposition does not appear in them until they are tempered [17,18]. The introduction of vanadium leads to less solute drag than other alloying elements [19,20]. It also seems to affect the deposition of other carbide-producing elements [21]. In other studies, rare earth elements have been mentioned as modifiers to enhance mechanical properties via melting purification and grain size optimization [21]. Rare earth elements perform the pinning process of the grain boundary instead of carbides by oxides and sulfides. The oxides and sulfides of these elements are formed in the early stages of casting and do not require secondary heat treatment for formation. Besides the mechanism of grain boundary pinning by oxides and sulfides, rare earth elements have a larger atomic radius than iron and can create extraordinary solute drag when placed in a chemical composition [22]. Finally, oxides such as Ce_2O_3 form during solidification, acting as heterogeneous nucleation sites. Rare earth elements are expected to play a desirable role in optimizing the properties of bainite steels. It is demonstrated that a modifier, including titanium, vanadium, and rare earth elements, significantly affects the mechanical properties, which is affected by the dendritic structure and segregation of the carbon and alloying elements, and by the austenite grains. However, from the few reports in the literature, most have focused on studying the influence of microalloying elements such as vanadium and rare earth on the microstructure and mechanical properties of carbide-free bainitic steels. Therefore, the purpose of the present investigation is to examine the effect of vanadium and rare earth on the structure, phase transformation kinetics, and mechanical properties of carbide-free bainitic steel containing silicon for obtaining a combination of strength and ductility along with low manufacturing costs.

2. Materials and Methods

All samples in this study were prepared by the casting and austempering process. Melts preparation was conducted using a carbon steel scrap, alloying elements and ferroalloys in an Inductotherm network frequency induction furnace with a capacity of 800 kg.

The optimal content of 0.1 wt% for vanadium was selected based on the research conducted by Ollilainen et al. [23], Kim et al. [24], and Yang et al. [25]. However, optimal content of 0.03 wt.% for rare earth was selected according to the studies of Adabavazeh et al. [26] and Ji et al. [27]. The chemical composition of the studied samples is listed in Table 1. The chemical composition of the samples was measured by a FOUNDRY-MASTER Pro2 optical emission spectrometer (OES). The casting procedure for all 1.6511, 1.6511Si2, 1.6511Si2M, and 1.6511Si2V specimens was conducted in sand molds prepared according to ASTM A781-05 style keel blocks (Figure 1a). A CFB matrix in the as-casted sample was achieved by using isothermal heat treatment in the lower bainite temperature range and adding 2 wt.% silicon to the matrix. The austempering process was carried out at 300 °C for 5 h in a KNO_3 salt bath and $NaNO_3$ with 50% of each salt. The heat treatment process cycle is shown in Figure 1b. For further studies, samples were machined from the tensile zone of the austempered keel blocks based on ASTM A781-05.

Table 1. Chemical composition of the studied samples and their identification code.

Sample Description	Identification Code	C	Si	Mn	V	RE	Cr	Mo	Ni
DIN 36CrNiMo4	1.6511	0.4	0.4	0.8	0	0	0.9	0.4	0.9
DIN 36CrNiMo4-2Si	1.6511Si2	0.4	2	0.8	0	0	0.9	0.4	0.9
DIN 36CrNiMo4-2Si-0.03RE	1.6511Si2M	0.4	2	0.8	0	0.03	0.9	0.4	0.9
DIN 36CrNiMo4-2Si-0.1V	1.6511Si2V	0.4	2	0.8	0.1	0	0.9	0.4	0.9

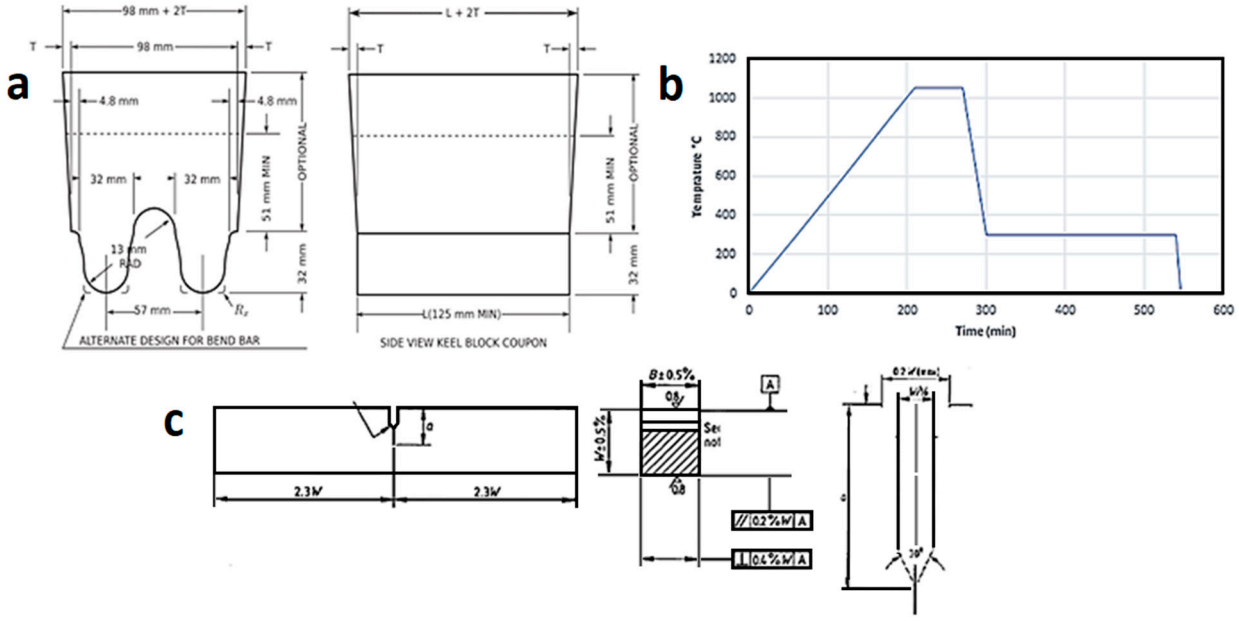

Figure 1. (**a**) Schematic of the keel blocks; (**b**) heat-treatment process cycle; and (**c**) CTOD samples.

To investigate the effect of alloying elements on the transformation kinetics, isothermal dilatometry was conducted on the as-cast samples using BAHR 805A/D dilatometry in cycles similar to Figure 1b. Continued cooling dilatometry was also performed to check the effect of alloying elements on the critical temperatures of all samples. An Olympus PME3 light microscope and TESCAN-LMU 30 kV electron microscope equipped with energy-dispersive X-ray spectroscopy (EDS) were used to study the microstructure, and working distances were 4–5 mm. The ASTM E3-11(2017) standard was used for the preparation of metallographic specimens. Sample preparation was started by a mechanically wet grounding with 80–2500 SiC grit paper; subsequently, a 0.05 microns diamond polishing paste was employed for final preparation. The specimens were etched in 4% Nital solution (4% nitric acid + 96% ethanol) for 5 s. Phase composition of the matrix characterization was performed using X-ray diffraction (XRD) and electron backscatter diffraction (EBSD). A

Philips PW 1710 diffractometer, with its tube anode being Cu with Kα = 1.54242 Å, was used for the XRD analysis. The angle of the goniometer was selected from 20 to 120 degrees to include all the main steel peaks. XRD results were also analyzed by Xpert high score software. The EBSD was performed with an EDAX EBSD detector. Hardness tests were performed by Koppa Brinell (Universal), the tensile tests by GOTECH The AI-7000-LAU TESTING MACHINES at a 2 mm/min elongation rate at ambient temperature, and the Charpy impact at ambient temperature, according to the ASTM E23-2a standard, to evaluate the mechanical properties of the samples. Each test was repeated three times to examine the reproducibility of the results. CTOD sample preparation was performed according to the BS 7448-1 standard with a square cross-section. The groove shape profile was also prepared using a wire-cut according to Figure 1c, and the tip radius was considered to be 0.1 mm. The groove length was considered equal to 0.47 of the sample width. The Instron universal testing machine created the initial fatigue crack in the form of a three-point flexural.

3. Results and Discussion

3.1. Microstructural Evolution and Transformation Kinetics

Figure 2 shows the SEM metallography of 1.6511 steel in two-state, optimized states by adding 2 wt% silicon and the standard composition. The optimized silicon sample has a carbide-free bainite structure.

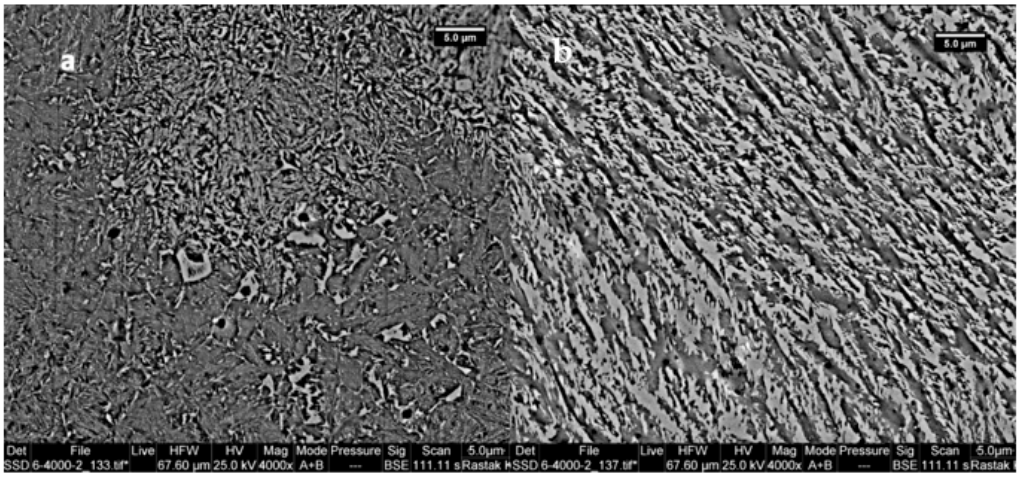

Figure 2. Microstructure of 1.6511: (**a**) standard composition and (**b**) optimized states by adding 2 wt% silicon. Note: The microstructure has changed from martensitic bainitic to CFB with the addition of silicon.

XRD results (Figure 3) show that in the pattern of the standard WN 1.6511 sample a cementite peak presents, but due to the small dimensions of the carbides, the peak intensity is low and wide (indicated by the circle in Figure 3). In contrast, this peak is removed in the optimized sample. Matching these patterns by the SEM images (Figure 2), it can be concluded that the structure of the optimized sample consists only of bainitic ferrite and austenite, or in other words, carbide-free bainite. In the following, the effects of adding alloying elements to this CFB matrix are examined.

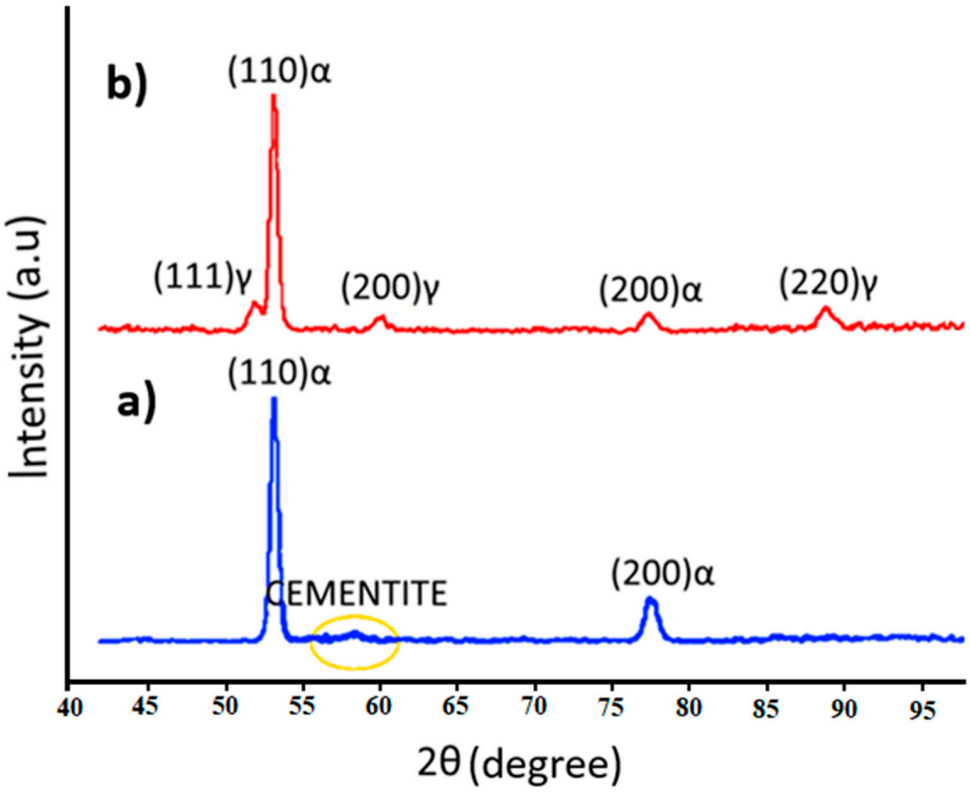

Figure 3. XRD patterns of (**a**) the 1.6511 sample and (**b**) the silicon-modified (1.6511Si2) sample austempered at 300 °C. Note: The cementite peak vanishes when adding silicone.

Figure 4 presents the dilatometric test results of samples with different chemical compositions, including the silicon-modified alloy (1.6511Si2) and silicon-modified alloy after adding 0.1 wt% of vanadium (1.6511Si2V), as well as the silicon-modified alloy after adding 0.03 wt% of rare earth alloy (1.6511Si2M) at a continuous cooling rate of 4 °C/s. In the 1.6511Si2 sample, three transformations peaks are observed at temperatures of 556.55, 437.9, and 282.4 °C, which are related to the transformation of austenite to perlite (or ferrite), bainite, and martensite, respectively, according to the temperature range. After adding vanadium to the chemical composition, the transformation of austenite to perlite (or ferrite) did not occur, and the temperatures of the bainite and martensitic transformations were transferred to lower temperatures. A similar behavior is observed after the addition of cerium to the chemical composition. The peak associated with the perlite (or ferrite) transformation was removed; in other words, due to the addition of both microalloy elements, the critical cooling rate for the formation of diffusionless transformations was reduced. However, unlike vanadium, cerium and lanthanum have increased the initiation temperature of the martensitic transformation (Ms in the 1.6511Si2 sample is 282.4 °C, in the 1.6511Si2V sample it is 230 °C, and in the sample containing the rare earth element it is 290 °C). In other words, with the addition of rare earth elements (cerium and lanthanum), the process length for the bainite formation becomes shorter. Microscopic studies (Figure 5) show that the microstructure after adding vanadium and rare earth elements is in the form of granular bainite. However, in samples containing vanadium, this granular bainite is carbide-free; however, in the sample containing rare earth elements, the formation of carbide phases in the microstructure was not prevented. No perlite formation in the structure of samples containing microalloying elements led to carbon retained in the chemical composition of the parent phase (austenite), and it could be more thermodynamic stable at lower temperatures. The shifting of the bainite transformation temperature to lower temperatures in both samples can be due to this issue, along with increasing the strength of the matrix phase due to the solid solution strengthening effect. However, because of the formation of carbide in the sample containing cerium and lanthanum in

the bainite transformation, the carbon content of the parent phase has decreased, and as a result, its thermodynamic stability has decreased, and martensitic transformation occurred at higher temperatures than the vanadium-containing sample.

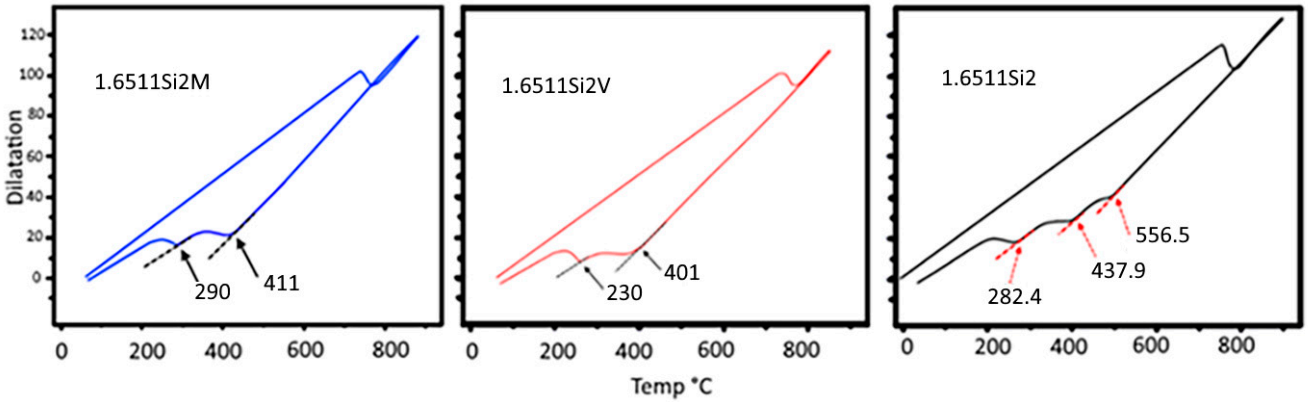

Figure 4. Dilatometric test results of the silicon-modified alloy (1.6511Si2), silicon-modified alloy after adding vanadium (1.6511Si2V), and silicon-modified alloy after adding a rare earth alloy (1.6511Si2M) at a continuous cooling rate of 4 °C/s.

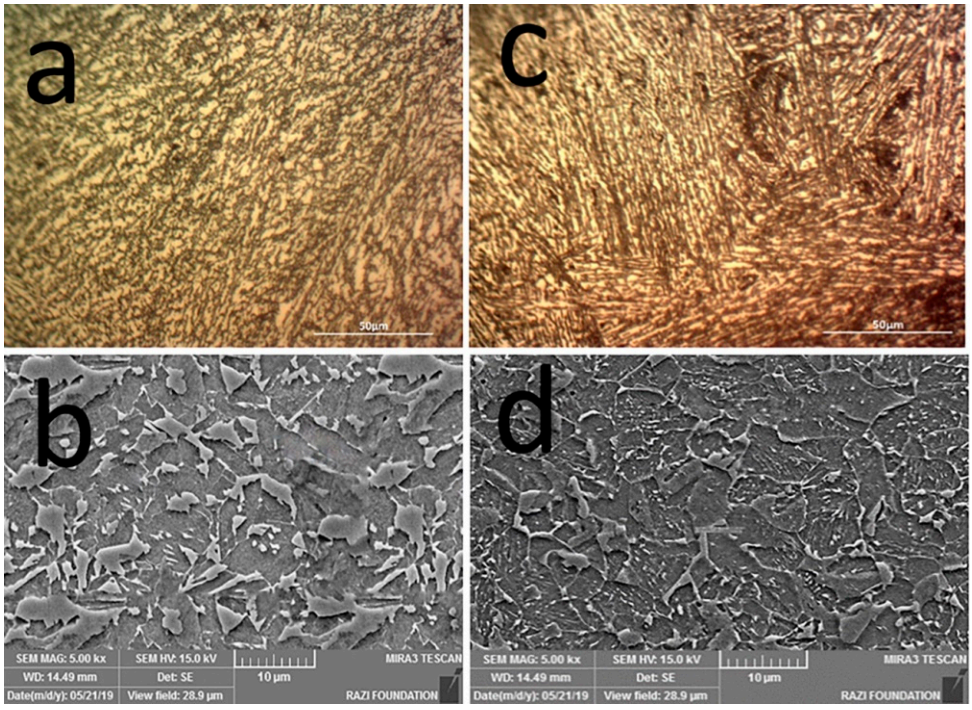

Figure 5. (**a**) Optical microscopy and (**b**) SEM metallography of sample 1.6511Si2V; (**c**) optical microscopy and (**d**) SEM metallography of sample 1.6511Si2M. SEM metallography shows that the microstructure of both alloys is granular bainite. Note: 1.6511Si2V is CFB while 1.6511Si2M is containing carbides.

It has been confirmed in various studies [23,24,28] that with an increasing vanadium content, the rate of perlite transformation slows and the steel hardness increases by increasing the vanadium content. Vanadium in solution seems to affect the mobility of the carbon atoms [10,25–30]. Using Thermo-Calc software we performed the thermodynamic analysis, showing that the type of stable carbides in the matrix changes from cementite to M_6C and M_7C_3 carbides. The formation of these carbides is due to the uphill diffusion of elements such as cerium and molybdenum [31]. Therefore, the formation kinetics of these carbides will be slower than cementite, and at low temperatures of transformation,

the possibility of their formation is very low. The presence of cerium and lanthanum in a chemical composition similar to vanadium increases the probability of obtaining bainite, and especially martensite, at lower cooling rates. The reason for this manner in different studies has been stated as the deposition of this element in the interface of ferrite and austenite, which prevents the diffusion of carbon [30–33].

Preventing or disrupting the diffusion of carbon by vanadium and cerium can be the main reason for the delay in forming the perlite (or ferrite). However, in general, the behaviors of the two elements are different. Vanadium retains carbon in austenite, while cerium prevents the diffusion of trapped carbon in ferrite into austenite. Thus, the probability of cementite formation in the sample containing cerium is much higher than the sample containing vanadium. This issue will be discussed in further discussions. Isothermal dilatometry at 300 °C was used to investigate the effect of vanadium and cerium on the transformation in the isothermal condition (Figure 6). Time was measured till the dilatation stopped. In this respect, vanadium leads to an earlier cessation of transformation, and cerium delays its cessation by a different behavior; therefore, in similar conditions, the specimen that contains the vanadium parent phase should have a greater effect on the isothermal transformation than a specimen that contains rare earth elements. This point is confirmed by other examinations in the present study. Microscopic images in Figure 7 show that the substructure resulting from the isothermal transformation in both samples is carbide-free bainite. The retained austenite phase percentage change with increasing vanadium and rare earth elements was investigated using the EBSD phase map. According to the phase map (Figure 8), the face-centered cubic (FCC) phase corresponding to austenite is shown in a different color from the body-centered cubic (BCC) phase corresponding to the ferrite phase. Image analysis showed the volume percent of retained austenite in sample 1.651i2 is about 16%. The sample containing vanadium and cerium have 20 and 12% volume fractions of austenite, respectively. As expected, the retained austenite volume fraction is higher in the sample where the bainite transformation stopped earlier (1.6511Si2V sample), and the volume fraction of the retained austenite is lower in the sample where the transformation stopped posteriorly (1.6511Si2M sample).

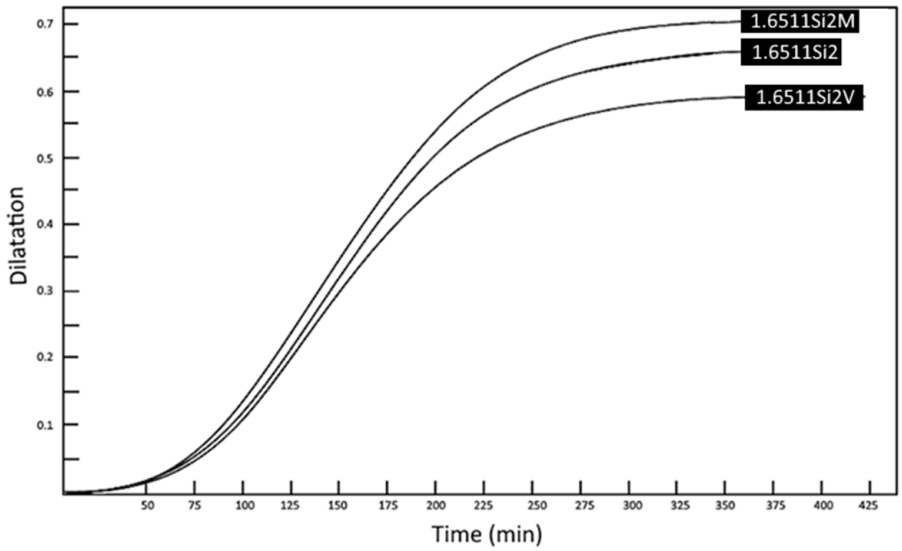

Figure 6. Isothermal dilatometry graph of 1.6511Si2, 1.6511Si2V, and 1.6511Si2M at 300 °C. Note: Transformation cessation is delayed by adding rare earth elements, but vanadium caused it to occur sooner.

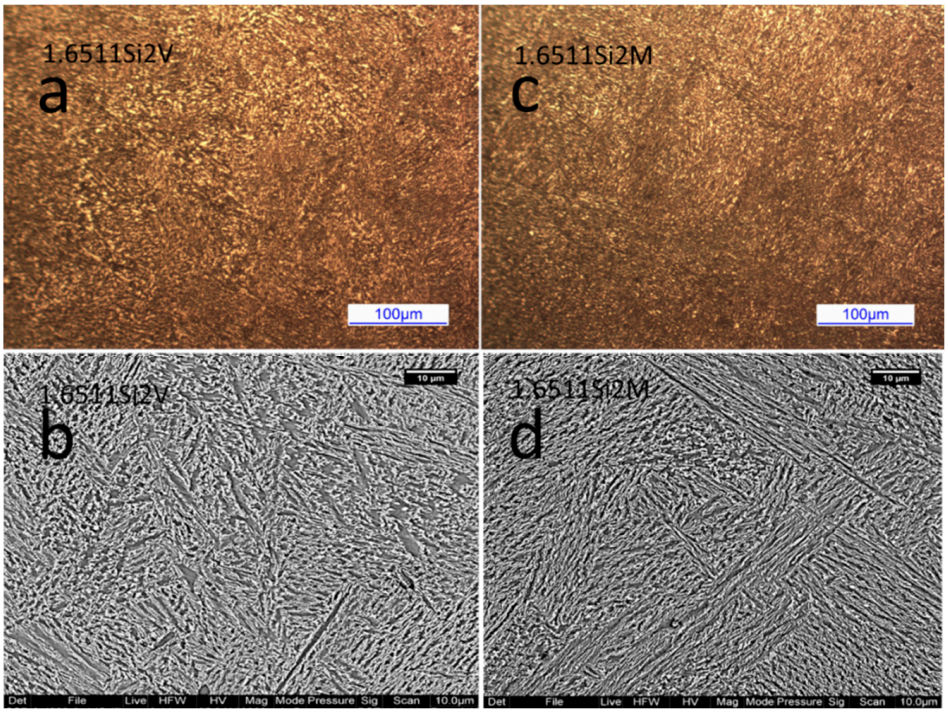

Figure 7. Optical and electron metallography of 1.6511Si2V (**a**,**b**) and 1.6511Si2M (**c**,**d**) after austempering at 300 °C. Note: All samples have CFB matrix.

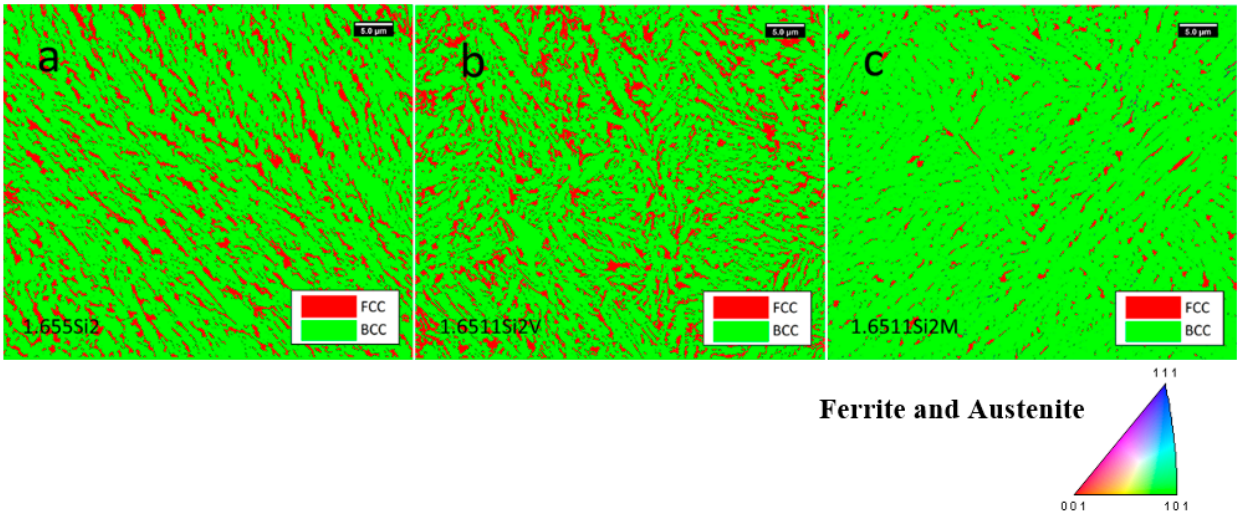

Figure 8. EBSD phase map of the (**a**) 1.6511Si2, (**b**) 1.6511Si2V, and (**c**) 1.6511Si2M samples. The red phase shows the retained austenite. Note: Retained austenite increased with vanadium and decreased with the rare earth elements.

Some of the observed changes in microstructure by the addition of these alloying elements could be due to changes in the activity of carbon by incorporating them, so the effect of these elements on carbon was investigated. The linear EDS method was employed to examine the effects of the addition of alloying elements on the carbon content of the austenite interface, as presented in Figure 9. The EDS analysis is not accurate enough to detect the carbon content, and thus only qualitatively employed it.

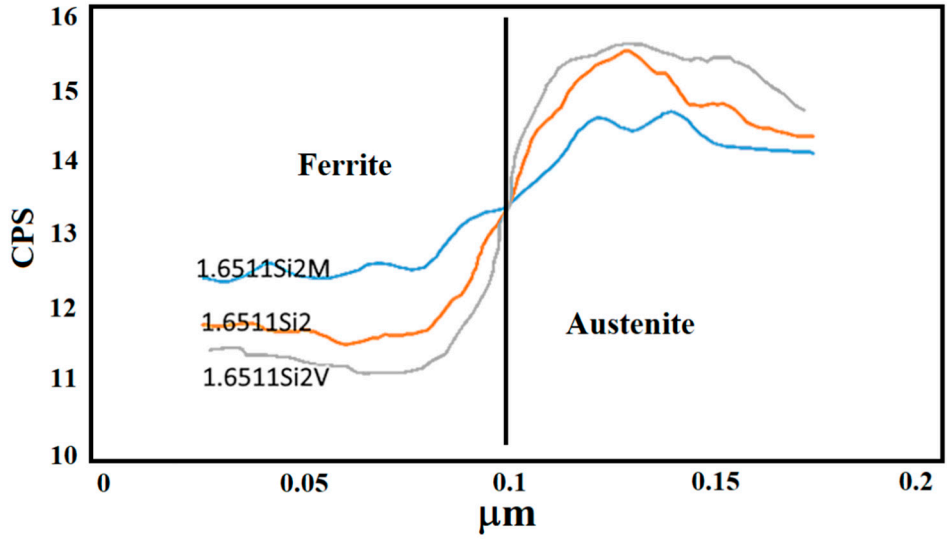

Figure 9. Linear EDS graph of the carbon content in 1.6511Si2, 1.6511Si2V, and 1.6511Si2M.

It is observed that by adding vanadium, carbon has a higher tendency to remain in austenite, and the average carbon content of austenite slightly increases by the addition of vanadium. Unlike vanadium, the presence of cerium and lanthanum in the CFB matrix increases the carbon content in ferrite and decreases it in austenite. If the EDS results are correct, it is possible to investigate the reason for the earlier or later cessation of the bainite transformation by adding alloying elements. Bainite transformation takes place as long as the thermodynamic conditions are possible to convert austenite into bainite. By decreasing the stability of austenite, bainite transformation needs less activation energy. So, in equal temperature in the alloy, its matrix austenite stability is less; hence, the bainite transformation progresses more. One of the important items that austenite stability depends on is carbon content. Decreasing carbon content resulted in austenite becoming unstable, so it can be concluded that bainite transformation can be assisted by an alloying element that reduces the carbon content of austenite. In this regard, rare earth elements assist bainite transformation, while vanadium postpone this transformation. In other words, vanadium assisted carbon diffusion, but rare earth elements act as a barrier to diffusion. Figure 10 shows the prior austenite grain size measured using EBSD analysis. Comparing Figure 10a–c shows that the addition of vanadium into the CFB steels leads to the escalation of the grain size of the PAG from an average of 15 µm to 30 µm, while the average grain size of PAG was reduced to about 7 µm by the addition of rare earth elements.

Grain growth with the addition of vanadium contradicts the results of many scientific studies and the reason for the use of vanadium in tool steels [34,35]. Grain growth due to the addition of vanadium is observed in only a few studies [11,30]. Therefore, the lack of information in this regard is quite noticeable. Based on the points presented in [11,30], it seems that encapsulation of vanadium into the CFB steel prevented the formation of carbide phases; it also disrupted the formation of other nitrites and oxides. Lack of oxides and carbides that act as barriers to grain growth will lead to grain growth. The rare earth elements usually prevent grain growth due to segregation in the interfaces of austenite and ferrite [36]. These elements can form oxidation and nitride phases with very high stability during solidification, and these oxides and nitrides act as heterogeneous nucleation sites during solidification [37]. During solidification, rare earth elements increase the volume fraction of the equiaxed zone by changing the surface tension of the solidification phases and reducing the distance dendrite arm spacing (DAS) [38]. All of the above could have occurred due to the steel under study, which resulted in fine-grained and microstructure modification. According to the study by Chester and Bhadeshia [39], the reduction in the grain size of the steel results in increasing the number of nucleation sites in bainite, thereby increasing the volume fraction of the bainite during bainitic transformation, which

is consistent with the results of the dilatometry and EBSD test in the previous section. The formation of carbide in the microstructure of the alloy that contains rare earth elements could also reduce the grain size. Due to the finer grain size, the diffusion coefficient and, as a result, the mobility of silicon in the structure increases [40]. In other words, the probability of trapping this element in cementite decreases as the grain size decreases. On the other hand, increasing the ferrite carbon content decreases its thermodynamic stability, and the tendency to form carbide (cementite) increases. Therefore, by adding rare earth elements to the CFB matrix, the probability of carbide formation increases.

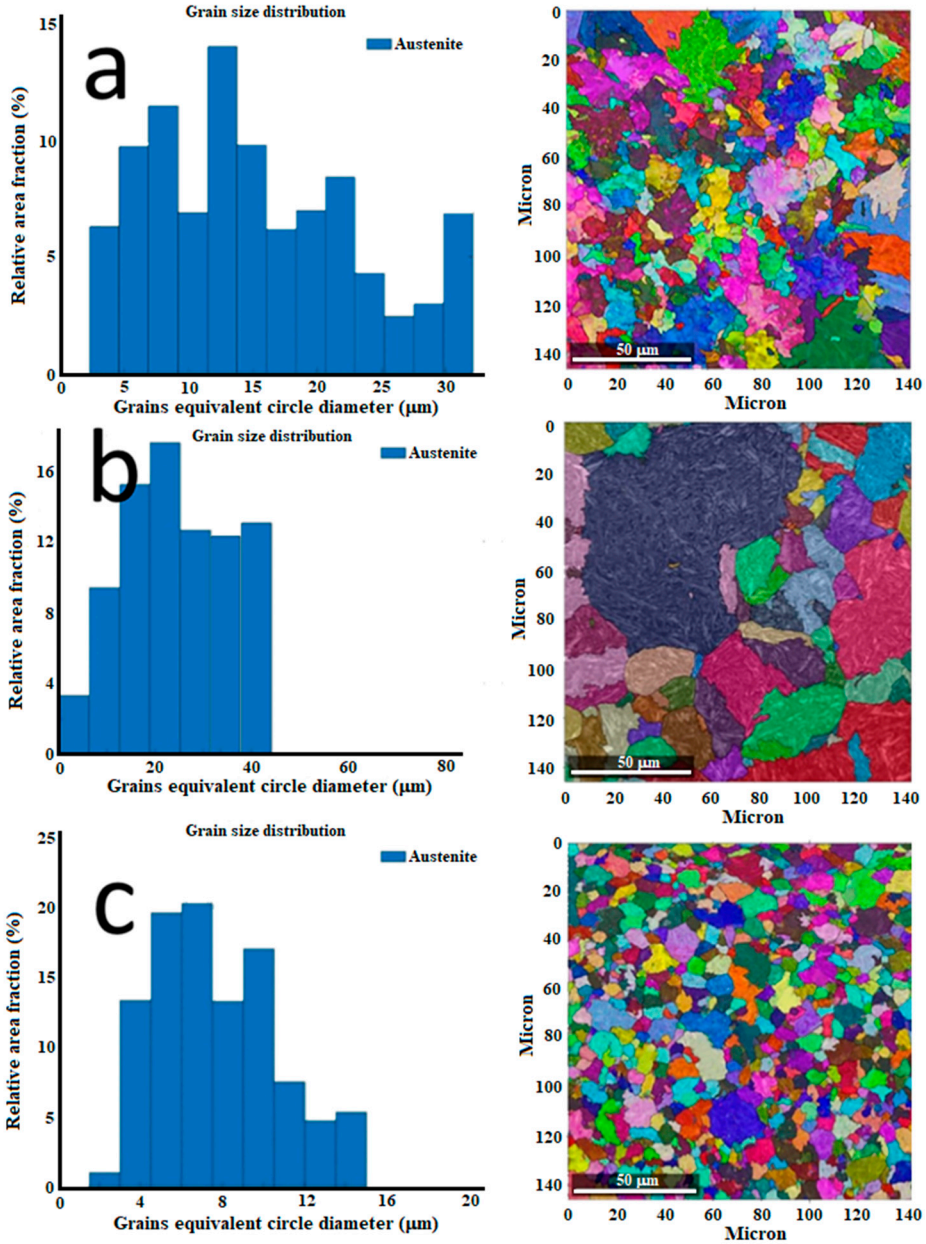

Figure 10. EBSD images of the PAG distribution of (**a**) 1.6511Si2, (**b**) 1.6511Si2V, and (**c**) 1.6511Si2M. By adding vanadium to the chemical composition the PAG size increased and by adding a rare earth element it decreased.

3.2. Mechanical Properties

Figure 11 shows the hardness graph of the studied samples in the standard state after the addition of silicon and obtaining the CFB structure and the microalloyed CFB samples. The Brinell hardness value in the standard sample (without silicon) was 380 HB, which

increased to 410 HB with the addition of silicon due to the solid solution strengthening and microstructure change to CFB. Comparing the hardness of other microalloyed samples with this sample, it seems that the hardness value depends on the amount of retained austenite in the matrix. In sample 1.6511Si2V, with the higher amount of retained austenite, a lower hardness value was measured (405 HB), and in sample 1.6511Si2M, with lower retained austenite, a higher hardness value (415 HB) was observed.

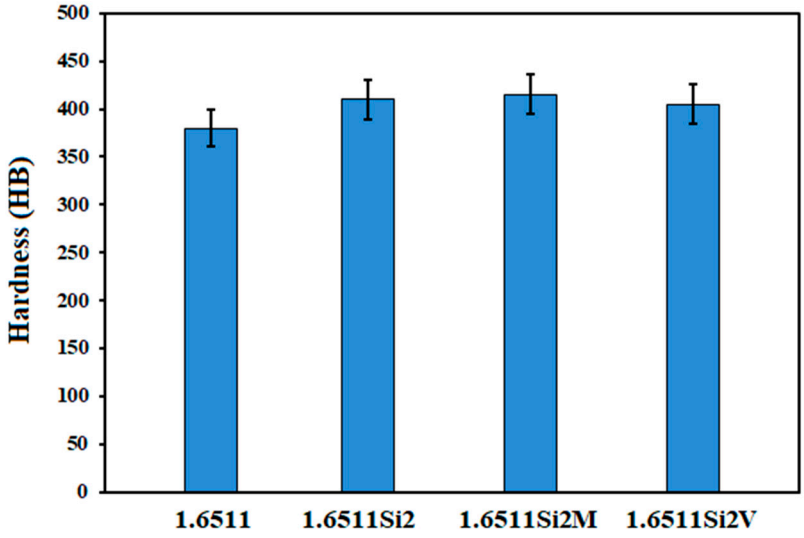

Figure 11. Variation in the hardness of the samples based on their identification codes.

Figure 12 demonstrates the engineering stress–strain curve and Table 2 shows the 0.2% offset yield and tensile strength of the studied samples. The yield strength of all specimens mainly followed the Hall Patch relationship [40]. The 1.6511Si2M sample with an average PAG size of 7 μm showed an average yield strength of 878 MPa, and the 1.6511Si2V sample with an average PAG size of 30 μm showed a yield strength of 787 MPa. It should be noted that the standard tensile strength is also affected by the matrix structure and solid solution strengthening. The lower yield stress of the standard samples, with an average grain size of 12 μm compared to other samples, especially 1.6511Si2 with a similar grain size (average 15 μm), is mainly due to the lack of silicon in the matrix of the base steel.

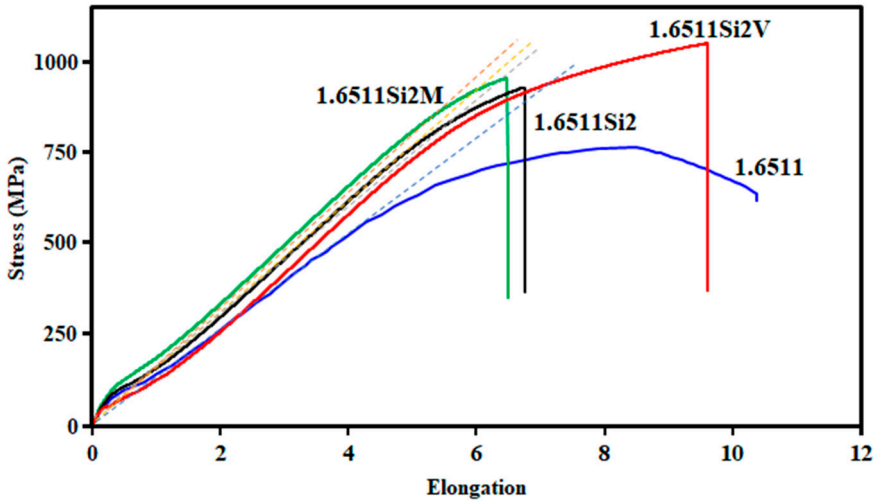

Figure 12. Typical engineering stress–strain curve of samples.

Table 2. Mechanical properties, including the yield stress (YS, with 0.2% offset) and ultimate tensile strength (UTS) of the samples.

Sample	Yield Strength (MPa)	Ultimate Tensile Strength (MPa)
1.6511	713 ± 3	915 ± 4
1.6511Si2	858 ± 4	965 ± 4
1.6511Si2M	878 ± 4	980 ± 4
1.6511Si2V	787 ± 3	1063 ± 5

Studies by Tao et al. [41] on duplex steels show that the elastic modulus of ferrite is higher than that of austenite. However, the austenite in these steels has a higher work hardening coefficient and tensile strength. Due to the higher percentage of retained austenite (about 20 vol%) in the microstructure of the 1.6511Si2V sample, the tensile strength and relative elongation are higher than the other samples (tensile strength in this sample is 1063 MPa, and the relative elongation is about 10%). Reducing the percentage of retained austenite in the 1.6511Si2M sample compared to the 1.6511Si2V sample from 20 to 12 vol% led to a 7% reduction in tensile strength to 980 MPa and a 3.5% reduction in elongation. It should be considered that despite the strong relationship between the tensile strength and the PAG size and the percentage of retained austenite in the matrix phase, other factors such as the grain boundary characteristics, the morphology of inclusions in the structure, and many other metallurgical variables can also affect the final properties of the steel. The behavior of the 1.6511Si2V sample in the tensile test indicates that despite a high amount of retained austenite in the matrix, they are not bulky and unstable, so they do not turn into untampered martensite due to applied stresses. The conversion of retained austenite to untampered martensite can cause a reduction in the ultimate tensile strength (UTS) from 1063 ± 5 MPa for the 1.6511Si2V sample to 965 ± 4 MPa for the 1.6511Si2 sample, as presented in Figure 12. On the other hand, stable retained austenite can increase the tensile strength in two ways: crack blinding and TRIP [37]. The SEM image shows the fracture surfaces of 1.6511Si2 after impact testing, as shown in Figure 13. It is worth noting that both phenomena are likely to occur together where the presence of dimples (Figure 13a) is related to the existence of a soft phase, while the crack closure is associated with the TRIP phenomenon (Figure 13b).

Figure 14 shows the variation in the energy-absorbed values attained from the impact test of the 1.6511, 1.6511Si2, 1.6511Si2V, and 1.6511Si2M samples. Impact testing is an indirect method for obtaining fracture toughness [42,43]. Since the fracture toughness mostly depends on the possibility of blinding the crack tip by secondary phases and changing the crack path due to grain boundaries [44], the impact test results of the samples, shown in Figure 14, were studied from these two perspectives. Sample 1.6511Si2V has the highest volume fraction of retained austenite among the samples; despite the larger grain size due to the possibility of simultaneous blinding and the TRIP phenomenon resulting from its retained austenite, it was able to absorb great energy before failure. Rare earth elements, besides decreasing the grain size, which leads to increased fracture toughness [45–52], also increase the grain boundary strength [36]. It seems that there is an increase in energy required for the fracture of the 1.6511Si2M sample compared to the standard sample, and the 1.6511Si2 sample has a higher grain boundary volume and higher grain boundary strength compared to other samples. Moreover, the rare earth elements reduce the distance between the dendritic arms, leading to improved mechanical properties regardless of other cases [38]. The 1.6511 sample in the standard state (without Si) absorbs the lowest amount of energy before fracture, which can be due to the simultaneous lack of retained austenite (or in other words, CFB matrix) and the presence of carbide in the structure.

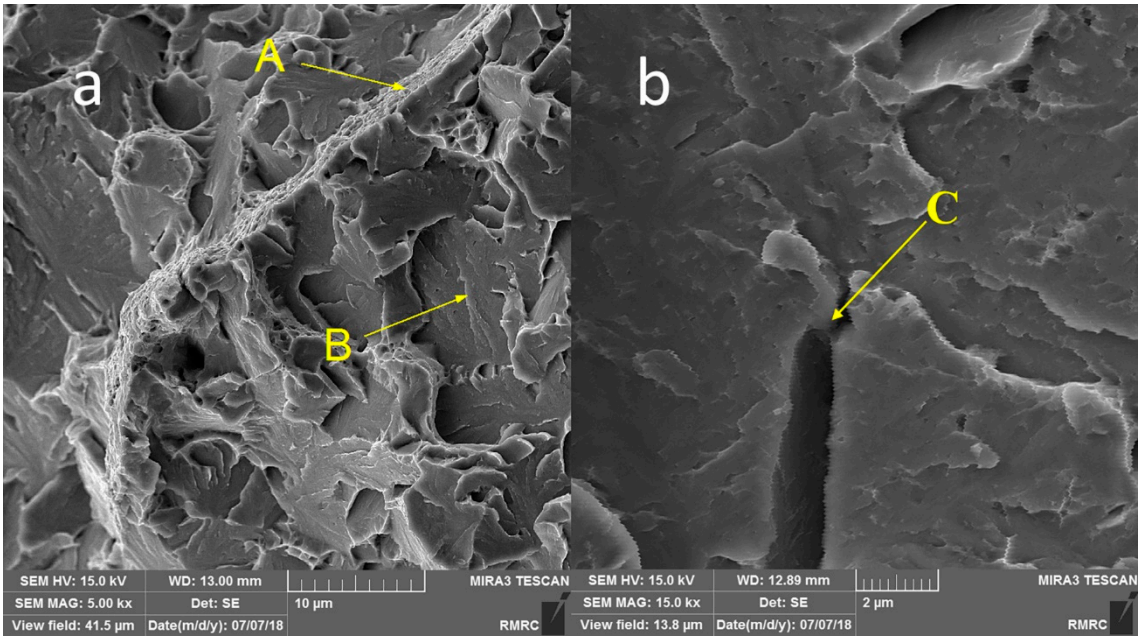

Figure 13. SEM images of the fracture surfaces of 1.6511Si2 after impact testing (**a**) two different fracture surfaces, a ductile fracture (dimples in A area) and brittle crack face (B area); and (**b**) crack blunting by the second phase (C area).

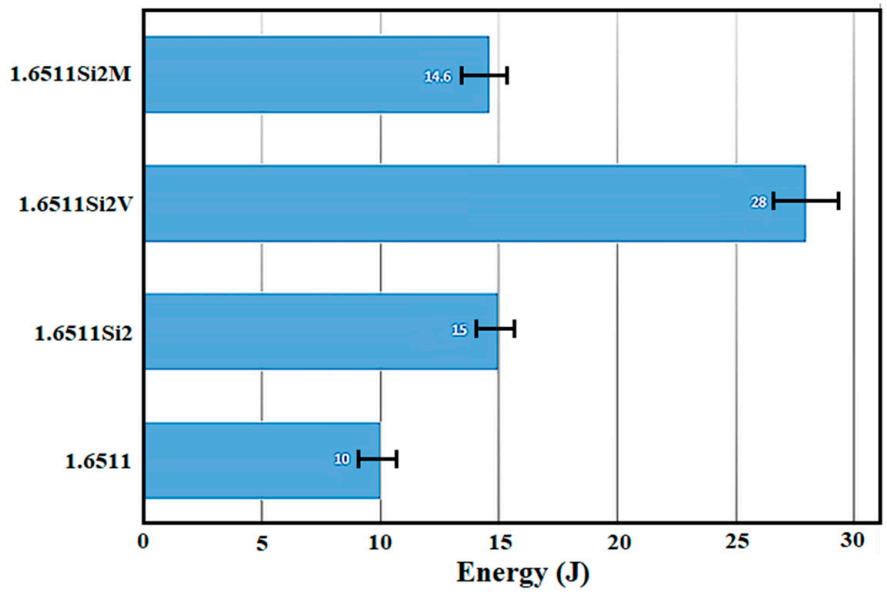

Figure 14. Graph of the energy absorbed during the impact test of the samples.

3.3. CTOD Examination and Failure Mechanism

According to the results of the CTOD test, the Kq of the samples increased from 37.53 MPa $m^{1/2}$ (For 1.6511) to 54.9 MPa $m^{1/2}$ (for 1.6511Si2V). Figure 15 shows the force–crack tip opening displacement relationships for the 1.6511, 1.6511 Si2, and 1.6511Si2V samples. As can be seen in the figure, 1.6511Si2V experienced more force and aperture before failure than the other samples. A very significant difference between the CFB samples graph is the existence of a pop-up in the stages before the failure. The leap in the graph indicates an increase in the fracture toughness of the sample due to the TRIP phenomenon during loading. The pop-up amount increased by increasing the amount of retained austenite.

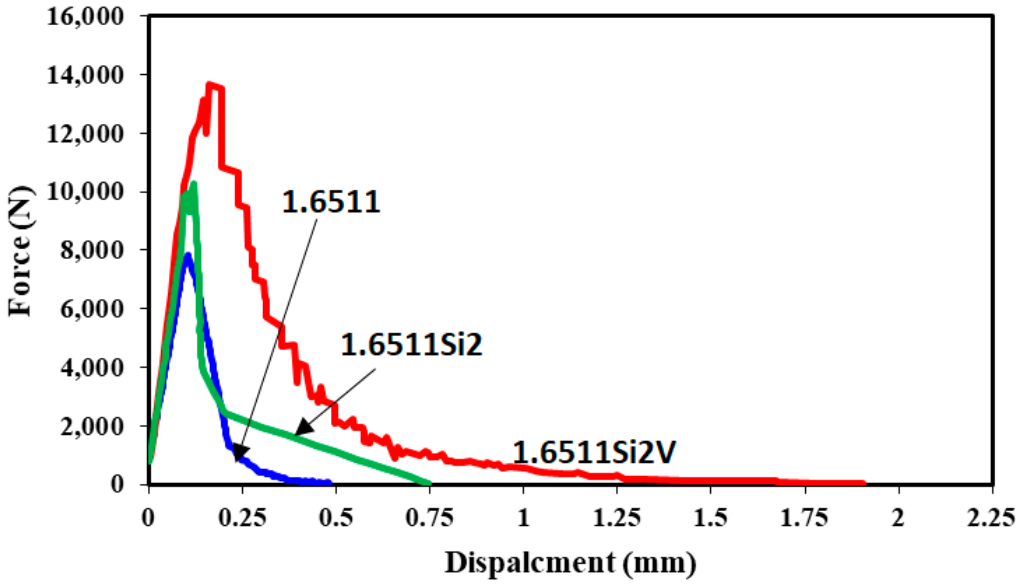

Figure 15. Force against the opening of the crack tip opening displacement of sample 1.6511 (blue), 1.6511 Si2 (green), and 1.6511Si2V (red).

Figure 16 and Table 3 show the average length of the crack. In the vanadium-containing specimen, the average length of the crack growth zone is 9.56 mm, while in other specimens it is more than 10.2 mm. The variation in crack length is lower in samples containing more silicon. It shows that more retained austenite causes a lower crack growth length.

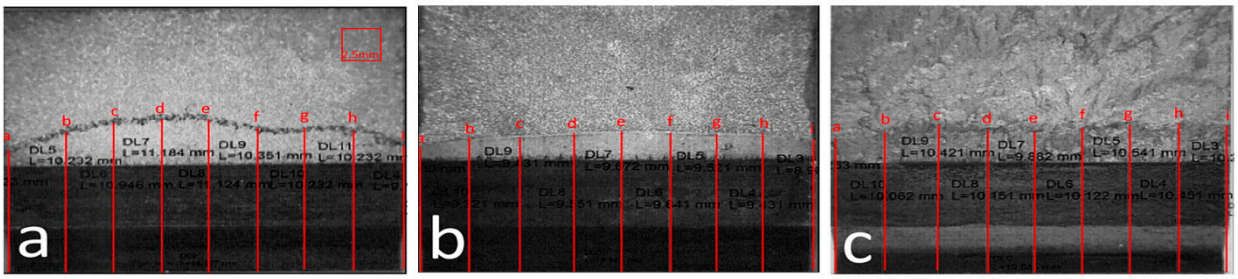

Figure 16. Cross section of the CTOD sample fracture surfaces and length of the crack (a to i) for (**a**) 1.6511, (**b**) 16511Si2V, and (**c**) 1.6511Si2. Note: In CFB samples, the crack lengths are more uniform compared with the no CFB sample.

Table 3. Crack length of the sample after failure in the CTOD test.

Sample	Crack Length in Zone a (mm)	Crack Length in Zone b (mm)	Crack Length in Zone c (mm)	Crack Length in Zone d (mm)	Crack Length in Zone e (mm)	Crack Length in Zone f (mm)	Crack Length in Zone g (mm)	Crack Length in Zone h (mm)	Crack Length in Zone I (mm)
1.6511	8.923	10.232	10.949	11.184	11.124	10.351	10.232	10.232	9.131
1.6511Si2V	9.276	9.486	9.605	9.605	9.755	9.575	9.755	9.545	9.426
1.6511Si2	9.253	10.062	10.421	10.151	9.882	10.122	10.541	10.541	10.271

The crack length in the silicon sample is not much different from that in the sample without Si, and since the sample matrix contains CFB silicon, it seems illogical to consider crack blindness as the main mechanism for increasing the resistance in samples with a CFB matrix. On the other hand, the existence of significant pops-up and an increase in force for the same displacement in steels with a CFB matrix compared to non-CFB matrix steels can be attributed to two phenomena. One is the increase in strength due to the solid solution as

a result of the increase in silicon, and the other is the TRIP phenomenon. On the other hand, due to the slight increase in vanadium content in the 1.6511Si2V sample, the increase in the probability of the TRIP phenomenon occurring with the increase in retained austenite can be considered as the main factor of resistance to crack growth.

4. Conclusions

(1) Adding vanadium to the chemical composition increases the possibility of producing a CFB matrix, even in continuous cooling. On the other hand, by assisting the growth of PAG (in solid solution), it increases the volume fraction of retained austenite.

(2) Rare earth elements, due to their large atomic radius, can act like inclusions in the microstructure; even if they do not form oxides and sulfides, they lead to a reduction in grain size. These elements can cause carbide formation in ferrite by keeping more carbon in it. The encapsulation of Ce-La into the CFB matrix leads to a reduction in the grain size of the prior austenite by half, which resulted in a 25 vol% reduction in the retained austenite.

(3) The mechanical properties of CFB steels are mainly affected by the retained austenite content in the microstructure and its stability. For example, less than 4 vol% of retained austenite remaining in the 1.6511Si2M sample compared to the 1.6511Si2V sample resulted in a 7% reduction in tensile strength and a 3.5% reduction in elongation.

Author Contributions: Conceptualization, visualization, investigation, writing—original draft preparation, B.G.; Conceptualization, supervision, writing—review and editing, M.K.-A., K.A., H.G. and H.R.B.-R.; visualization, writing—review and editing, funding acquisition F.B. All authors have read and agreed to the published version of the manuscript.

Funding: This research received no external funding.

Institutional Review Board Statement: Not applicable.

Informed Consent Statement: Not applicable.

Data Availability Statement: All data provided in the present manuscript are available to whom it may concern.

Conflicts of Interest: The authors declare that they have no competing/financial conflict of interest in this paper.

References

1. Sandvik, B.P.J.; Nevalainen, H.P. Structu re-property relationships in commercial low-alloy bainitic-austenitic steel with high strength, ductility, and toughness. *Met. Technol.* **1981**, *8*, 213–220. [CrossRef]
2. Caballero, F.G.; Bhadeshia, H.; Mawella, K.J.A.; Jones, D.G.; Brown, P. Very strong low temperature bainite. *Mater. Sci. Technol.* **2002**, *18*, 279–284. [CrossRef]
3. Bhadeshia, H. *Bainite in Steels: Transformation, Microstructure and Properties*; IOM: Grand-Saconnex, Switzerland, 2001; ISBN 9780750680844.
4. Garcia-Mateo, C.; Caballero, F.G.; Bhadeshia, H. Low temperature bainite. *J. Phys. IV* **2003**, *112*, 285–288. [CrossRef]
5. Bhadeshia, H.K.D.H.; Edmonds, D.V. Bainite in silicon steels: New composition–property approach Part 1. *Met. Sci.* **1983**, *17*, 420–425. [CrossRef]
6. Khare, S.; Lee, K.; Bhadeshia, H. Carbide-free bainite: Compromise between rate of transformation and properties. *Metall. Mater. Trans. A* **2010**, *41*, 922–928. [CrossRef]
7. Moghaddam, P.V.; Prakash, B.; Vuorinen, E.; Fallqvist, M.; Andersson, J.M.; Hardell, J. High temperature tribology of TiAlN PVD coating sliding against 316L stainless steel and carbide-free bainitic steel. *Tribol. Int.* **2021**, *159*, 106847. [CrossRef]
8. Moghaddam, P.V.; Hardell, J.; Vuorinen, E.; Prakash, B. Effect of retained austenite on adhesion-dominated wear of nanostructured carbide-free bainitic steel. *Tribol. Int.* **2020**, *150*, 106348. [CrossRef]
9. Neog, S.P.; Bakshi, S.D.; Das, S. Effect of normal loading on microstructural evolution and sliding wear behaviour of novel continuously cooled carbide free bainitic steel. *Tribol. Int.* **2021**, *157*, 106846. [CrossRef]
10. Sourmail, T.; Otter, L.; Collin, S.; Billet, M.; Philippot, A.; Cristofari, F.; Secordel, P. Direct and indirect decomposition of retained austenite in continuously cooled bainitic steels: Influence of vanadium. *Mater. Charact.* **2021**, *173*, 110922. [CrossRef]
11. Sourmail, T.; Garcia-Mateo, C.; Caballero, F.G.; Cazottes, S.; Epicier, T.; Danoix, F.; Milbourn, D. The influence of vanadium on ferrite and bainite formation in a medium carbon steel. *Metall. Mater. Trans. A* **2017**, *48*, 3985–3996. [CrossRef]
12. Yu, X.; Wu, H.; Zhang, Y.; Yuan, R.; Gu, Y.; Feng, Y. Influence of niobium microalloying on the thermal stability of medium-carbon carbide-free bainitic steel. *J. Mater. Res. Technol.* **2021**, *12*, 487–499. [CrossRef]

13. Oblak, J.M.; Hehemann, R.F. *Transformation and Hardenability in Steels*; Climax Molybdenum Co.: Leadville, CO, USA, 1967; Volume 15.
14. Speer, J.; Matlock, D.K.; De Cooman, B.C.; Schroth, J.G. Carbon partitioning into austenite after martensite transformation. *Acta Mater.* **2003**, *51*, 2611–2622. [CrossRef]
15. Muddle, B.C.; Nie, J.F. Formation of bainite as a diffusional–displacive phase transformation. *Scr. Mater.* **2002**, *47*, 187–192. [CrossRef]
16. Saha, A.; Ghosh, G.; Olson, G.B. An assessment of interfacial dissipation effects at reconstructive ferrite–austenite interfaces. *Acta Mater.* **2005**, *53*, 141–149. [CrossRef]
17. Caballero, F.G.; Miller, M.K.; Babu, S.S.; Garcia-Mateo, C. Atomic scale observations of bainite transformation in a high carbon high silicon steel. *Acta Mater.* **2007**, *55*, 381–390. [CrossRef]
18. Hillert, M. The Nature of Bainite. *ISIJ Int.* **1995**, *35*, 1134–1140. [CrossRef]
19. García-Mateo, C.; López, B.; Rodriguez-Ibabe, J.M. Static recrystallization kinetics in warm worked vanadium microalloyed steels. *Mater. Sci. Eng. A* **2001**, *303*, 216–225. [CrossRef]
20. Glodowski, R.J. A review of vanadium microalloying in hot rolled steel sheet products. In Proceedings of the International Seminar 2005 on Application Technologies of Vanadium in Flat–Rolled Steels, Suzhou, China, 27–29 October 2005; pp. 43–51.
21. Lagneborg, R.; Siwecki, T.; Zajac, S.; Hutchinson, B. The role of vanadium in microalloyed steels. *Scand. J. Metall.* **1999**, *28*, 186–241.
22. Karasev, A.V.; Suito, H. Effects of oxide particles and solute elements on austenite grain growth in Fe–0.05 mass% C and Fe–10 mass% Ni alloys. *ISIJ Int.* **2008**, *48*, 658–666. [CrossRef]
23. Ollilainen, V.; Kasprzak, W.; Holappa, L. The effect of silicon, vanadium and nitrogen on the microstructure and hardness of air cooled medium carbon low alloy steels. *J. Mater. Process. Technol.* **2003**, *134*, 405–412. [CrossRef]
24. Kim, K.-S.; Du, L.-X.; Gao, C.-R. Influence of vanadium content on bainitic transformation of a low-carbon boron steel during continuous cooling. *Acta Metall. Sin.* **2015**, *28*, 692–698. [CrossRef]
25. Yang, B.; He, J.; Zhang, G.; Guo, J. *Vanadium*; Chapter 11—Applications of Vanadium in the Steel Industry; Elsevier: Amsterdam, The Netherlands, 2021; pp. 267–332. ISBN 978-0-12-818898-9.
26. Adabavazeh, Z.; Hwang, W.S.; Su, Y.H. Effect of adding cerium on microstructure and morphology of Ce-based inclusions formed in low-carbon steel. *Sci. Rep.* **2017**, *7*, 46503. [CrossRef] [PubMed]
27. Ji, Y.; Zhang, M.-X.; Ren, H. Roles of lanthanum and cerium in grain refinement of steels during solidification. *Metals* **2018**, *8*, 884. [CrossRef]
28. Gan, X.; Yang, G.; Zhao, G.; Mao, X.; Huang, H.; Xu, G. Effect of vanadium on the phase transformation behavior of Ti–Mo microalloyed ultra-high strength steel. *Steel Res. Int.* **2018**, *89*, 1800112. [CrossRef]
29. Han, C.F.; Sun, Y.F.; Wu, Y.; Ma, Y.H. Effects of vanadium and austempering temperature on microstructure and properties of CADI. *Metallogr. Microstruct. Anal.* **2015**, *4*, 135–145. [CrossRef]
30. Garcia-Mateo, C.; Morales-Rivas, L.; Caballero, F.G.; Milbourn, D.; Sourmail, T. Vanadium effect on a medium carbon forging steel. *Metals* **2016**, *6*, 130. [CrossRef]
31. Wieczerzak, K.; Bała, P.; Dziurka, R.; Tokarski, T.; Cios, G.; Kozieł, T.; Gondek, Ł. The effect of temperature on the evolution of eutectic carbides and M7C3→M23C6 carbides reaction in the rapidly solidified Fe-Cr-C alloy. *J. Alloys Compd.* **2016**, *698*, 673–684. [CrossRef]
32. Lin, Q.; Guo, F.; Zhu, X. Behaviors of lanthanum and cerium on grain boundaries in carbon manganese clean steel. *J. Rare Earths* **2007**, *25*, 485–489. [CrossRef]
33. Liang, Y.; Yi, Y.; Long, S.; Tan, Q. Effect of rare earth elements on isothermal transformation kinetics in Si-Mn-Mo bainite steels. *J. Mater. Eng. Perform.* **2014**, *23*, 4251–4258. [CrossRef]
34. Staśko, R.; Adrian, H.; Adrian, A. Effect of nitrogen and vanadium on austenite grain growth kinetics of a low alloy steel. *Mater. Charact.* **2006**, *56*, 340–347. [CrossRef]
35. Yazawa, Y.; Furuhara, T.; Maki, T. Effect of matrix recrystallization on morphology, crystallography and coarsening behavior of vanadium carbide in austenite. *Acta Mater.* **2004**, *52*, 3727–3736. [CrossRef]
36. Pan, F.; Zhang, J.; Chen, H.-L.; Su, Y.-H.; Kuo, C.-L.; Su, Y.-H.; Chen, S.-H.; Lin, K.-J.; Hsieh, P.-H.; Hwang, W.-S. Effects of rare earth metals on steel microstructures. *Materials* **2016**, *9*, 417. [CrossRef] [PubMed]
37. Weng, Y. *Ultra-Fine Grained Steels*; Springer Science & Business Media: Berlin, Germany, 2009; ISBN 3540772308.
38. Chen, X.; Li, Y. Fracture toughness improvement of austempered high silicon steel by titanium, vanadium and rare earth elements modification. *Mater. Sci. Eng. A* **2007**, *444*, 298–305. [CrossRef]
39. Chester, N.A.; Bhadeshia, H. Mathematical modelling of bainite transformation kinetics. *Le J. Phys. IV* **1997**, *7*, C5–C41. [CrossRef]
40. Porter, D.A. *Phase Transformations in Metals and Alloys (Revised Reprint)*; CRC Press LLC: Boca Raton, FL, USA, 2018; ISBN 9781138458079.
41. Tao, P.; Gong, J.; Wang, Y.; Jiang, Y.; Li, Y.; Cen, W. Characterization on stress-strain behavior of ferrite and austenite in a 2205 duplex stainless steel based on nanoindentation and finite element method. *Results Phys.* **2018**, *11*, 377–384. [CrossRef]
42. Roylance, D. *Introduction to Fracture Mechanics*; Massachusetts Institute of Technology: Cambridge, MA, USA, 2001.
43. Salemi, G.A. The effect of microstructure on estimation of the fracture toughness (KIC) rotor steel using Charpy absorbed energy (CVN). *J. Adv. Mater. Process.* **2013**, *1*, 11–17.

44. Wei, R.P. *Fracture Mechanics: Integration of Mechanics, Materials Science and Chemistry*; Cambridge University Press: Cambridge, UK, 2010; ISBN 1139484281.
45. Ali, M.; Nyo, T.; Kaijalainen, A.; Hannula, J.; Porter, D.; Kömi, J. Influence of chromium content on the microstructure and mechanical properties of thermomechanically hot-rolled low-carbon bainitic steels containing niobium. *Appl. Sci.* **2020**, *10*, 344. [CrossRef]
46. Borges, M.; Caldas, M.; Antunes, F.; Branco, R.; Prates, P. Fatigue crack growth from notches: A numerical analysis. *Appl. Sci.* **2020**, *10*, 4174. [CrossRef]
47. Su, L.; Xu, J.; Song, W.; Chu, L.; Gao, H.; Li, P.; Berto, F. Numerical investigation of strength mismatch effect on ductile crack growth resistance in welding pipe. *Appl. Sci.* **2020**, *10*, 1374. [CrossRef]
48. Honma, Y.; Sasaki, G.; Hashi, K. Effect of intercritical quenching temperature of Cu-containing low alloy steel of long part forging for offshore applications. *Appl. Sci.* **2019**, *9*, 1705. [CrossRef]
49. An, G.; Park, J.; Ohata, M.; Minami, F. Fracture assessment of weld joints of high-strength steel in pre-strained condition. *Appl. Sci.* **2019**, *9*, 1306. [CrossRef]
50. Antunes, F.; Santos, L.; Capela, C.; Ferreira, J.; Costa, J.; Jesus, J.; Prates, P. Fatigue crack growth in maraging steel obtained by selective laser melting. *Appl. Sci.* **2019**, *9*, 4412. [CrossRef]
51. Mudang, M.; Hamzah, E.; Bakhsheshi-Rad, H.R.; Berto, F. Effect of heat treatment on microstructure and creep behavior of Fe-40Ni-24Cr alloy. *Appl. Sci.* **2021**, *11*, 7951. [CrossRef]
52. Chen, D.; Cui, H.; Wang, R. High-temperature mechanical properties of 4.5%Al δ-TRIP Steel. *Appl. Sci.* **2019**, *9*, 5094. [CrossRef]